European Radiology (2019) 29:5635–5645
https://doi.org/10.1007/s00330-019-06155-2

HEAD AND NECK

Cervical necrotic lymphadenopathy: a diagnostic tree analysis model based on CT and clinical findings

Sung-Hye You[1] · Byungjun Kim[1,2] · Kyung-Sook Yang[3] · Bo Kyu Kim[1]

Received: 1 December 2018 / Revised: 22 February 2019 / Accepted: 11 March 2019 / Published online: 26 March 2019

Abstract

Objectives To establish a diagnostic tree analysis (DTA) model based on computed tomography (CT) findings and clinical information for differential diagnosis of cervical necrotic lymphadenopathy, especially in regions where tuberculous lymphadenitis and Kikuchi disease are common.

Methods A total of 290 patients (147 men and 143 women; mean age (years), 46.2 ± 19.5; range, 3–91) with pathologically confirmed metastasis ($n = 110$), tuberculous lymphadenitis ($n = 73$), Kikuchi disease ($n = 71$), and lymphoma ($n = 36$) who underwent contrast-enhanced neck CT were included. The patients were randomly divided into training (86%, 248/290) and validation (14%, 42/290) datasets to assess diagnostic performance of the DTA model. Two sorts of DTA models were created using a classification and regression tree algorithm on the basis of CT findings alone and that combined with clinical findings.

Results In the DTA model based on CT findings alone, perinodal infiltration, number of the necrotic foci, percentage of necrotic lymph node (LN), degree of necrosis, margin and shape of the necrotic portion, shape of the LN, and enhancement ratio (cutoff value, 1.93) were significant predictors for differential diagnosis of cervical necrotic lymphadenopathy. The overall accuracy was 80.6% and 73.8% in training and validation datasets. In the model based on imaging and clinical findings, tenderness, history of underlying malignancy, percentage of necrotic LN, degree of necrosis, and number of necrotic foci were significant predictors. The overall accuracy was 87.1% and 88.1% in training and external validation datasets.

Conclusions The DTA model based on CT imaging and clinical findings may be helpful for the diagnosis of cervical necrotic lymphadenopathy.

Key Points

- *The diagnostic tree analysis model based on CT may be useful for differential diagnosis of cervical necrotic lymphadenopathy.*
- *Perinodal infiltration, number of necrotic foci, percentage of necrotic lymph nodes, degree of necrosis, margin and shape of necrotic portion, lymph node shape, and enhancement ratio were the most significant predictors.*

Keywords Lymphadenopathy · Necrosis · Tuberculosis · Metastasis · Lymphoma

Electronic supplementary material The online version of this article (https://doi.org/10.1007/s00330-019-06155-2) contains supplementary material, which is available to authorized users.

✉ Byungjun Kim
cardillo@hanmail.net

[1] Department of Radiology, Korea University Hospital, Seoul, South Korea

[2] Department of Radiology, Anam Hospital, Korea University College of Medicine, #126-1, 5-Ka Anam-dong, Sungbuk ku, Seoul 136-705, South Korea

[3] Department of Biostatistics, College of Medicine, Korea University, Seoul, South Korea

Abbreviations

ADC	Apparent diffusion coefficient
CART	Classification and Regression Tree
CI	Confidence interval
CNB	Core needle biopsy
CT	Computed tomography
DTA	Diagnostic tree analysis
FNA	Fine needle aspiration
ICC	Intraclass correlation coefficient
KD	Kikuchi disease
LN(s)	Lymph node(s)
Necrotic LN_{per}	Percentage of necrotic lymphadenopathy
PACS	Picture archival and communication system
PCR	Polymerase chain reaction
ROI	Region of interest
TL	Tuberculous lymphadenitis

Introduction

Determining the etiology of cervical lymphadenopathy is challenging. Computed tomography (CT) plays a major role in the initial evaluation of patients with cervical necrotic lymph nodes (LN) as the pattern of necrosis reflects the pathologic features of the diseases [1]. While necrotic LN commonly corresponds to metastasis, lymphoma occasionally shows internal necrosis [2–4]. In a specific endemic area of tuberculosis and Kikuchi disease (KD), tuberculous lymphadenitis (TL) and KD involving cervical lymph nodes need to be included in the list of differential diagnoses [2, 4–6]. Although final diagnosis relies on histopathology [7], presumptive diagnosis based on CT is the key to improve treatment outcomes by orientating early management which could greatly differ according to presumptive diagnosis. For radiologically suspected TL, tuberculosis real-time polymerase chain reaction (PCR) assay for fine needle aspiration specimen is useful in diagnosis, and anti-tuberculosis medication is administrated after confirmation by pathology [8, 9]. In opposite, conservative management is the rule in KD because patients spontaneously recover within weeks or months [10, 11]. If CT shows lesions that are potentially metastasis, additional imaging workup is required to detect the primary site. For radiologically suspected lymphoma, a larger amount of core needle biopsy (CNB) specimen or excisional biopsy is necessary for immunostaining.

Extensive necrosis and calcifications are well-known imaging features of TL. Also, perinodal infiltration, minimal nodal necrosis, indistinct margin of necrotic foci, and higher CT density of nodal necrosis have been documented frequently in KD compared with TL [12, 13]. Eccentrically located necrotic portion and a relatively higher apparent diffusion coefficient (ADC) value of the that compared with benign LNs have been pointed out as characteristics of metastasis [3–5]; further, it has been documented that ADC values of the solid portion of involved LNs in lymphoma are lower than the values of metastatic or tuberculous LNs [4, 14]. However, there has been no study to establish the diagnostic tree for cervical necrotic lymphadenopathy. Therefore, the aims of our study were to compare CT findings of cervical necrotic LN in the case of metastasis, lymphoma, TL, and KD and to establish a diagnostic tree analysis (DTA) model utilizing CT findings in combination with clinical information for differential diagnosis in a region where tuberculosis and KD are prevalent.

Materials and methods

Patient selection

This retrospective study was approved by the institutional review board of our institution, and the requirement for informed consent was waived. From April 2010 to July 2018, 290 patients (147 men and 143 women; mean age, 46.2 ± 19.5 years; range, 3–91 years) who fulfill the following criteria were enrolled in the present study: (a) patients who underwent the contrast-enhanced neck CT for cervical lymphadenopathy less than 2 weeks before pathologic diagnosis; (b) radiologic report indicating the presence of the necrotic LN including the following terms: necrosis, necrotic, low density(ies), hypodensity(ies), foci of degeneration, non-enhancing portion, cystic degeneration; and (c) patients who were diagnosed with TL, KD, metastasis, or lymphoma through the fine needle aspiration (FNA), CNB, or excisional biopsy. Then, the patients were randomly divided into training (86%, 248/290) and external validation (14%, 42/290) datasets to test diagnostic performance of the DTA models (Fig. 1). Clinical characteristics including sex, age, history of underlying malignancy, presence of fever (body temperature ≥ 38 °C) and leukocytosis (WBC count ≥ 12,000), and methods of pathologic diagnosis (FNA, CNB, or excisional biopsy) were collected.

Image acquisition

CT images of four protocols (neck CT, oropharynx CT, larynx CT, and nasopharynx CT) consisted of contrast-enhanced axial and coronal images from the aortic arch to the skull base. CT examinations were performed using five different kinds of 64-multidetector row helical CT scanners (Brilliance 64 [64-channel], Ingenuity Core 128 [128-channel], and IQon Spectral CT [128-channel], Philips Healthcare; SOMATOM Definition Flash [64-channel] and SOMATOM Definition AS+ [64-channel], Siemens Healthineers). Scanning parameters were as follows: tube voltage, 120 kVp; effective tube current, 103–300 mA with dose modulation; field of view,

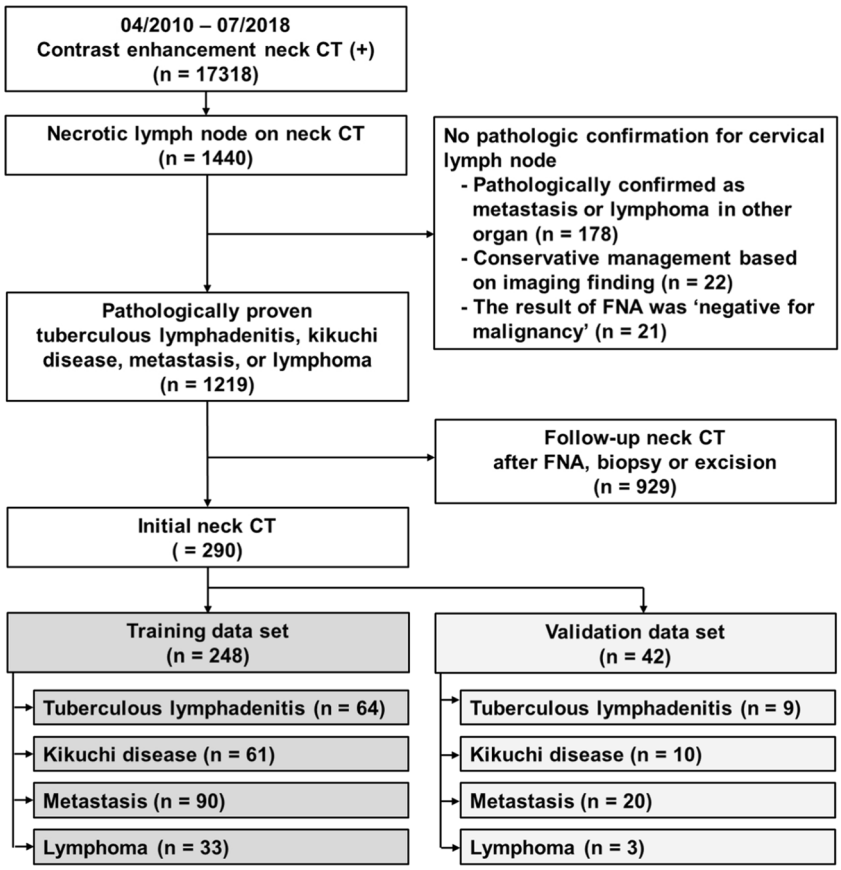

Fig. 1 Study design. CT, computed tomography

250 × 250 mm; matrix number, 512 × 512 pixels; collimation 64 × 0.625 mm; and reconstruction kernel algorithm, soft tissue. From the volumetric data, contiguous axial and coronal images were reconstructed at 3- or 2-mm intervals (3 mm, April 2010–June 2013; 2 mm, July 2013–July 2018). For each patient, iodinated contrast medium (Hexosure 300, LG Chem; Iomeron 300, Bracco; Pamiray 300, Dongkook Pharm; Xenetix 300, Guerbet; dose, 80–100 mL; rate, 2.5 mL/s) was administered, which was followed by a 20-mL saline flush using a power injector. Contrast-enhanced images were obtained with a delay of 60 s after the contrast injection. All scanning parameters are identical in the four protocols except for larynx CT (axial images with 1-mm intervals from the supraglottic to infraglottic area were additionally reconstructed in this protocol).

Image analysis

Axial and coronal neck CT images were reviewed using picture archival and communication system (PACS) with a fixed soft-tissue window setting (window level of 45 and width of 440). Imaging analysis was performed by two radiologists (S-H. Y. and BKK with 7 and 8 years' experience) independently and supervised by an expert radiologist (B. J. K. with 12 years' experience). The reviewers were blinded to the clinical history of patients and the final pathologic diagnosis of the lymphadenopathy.

Cervical lymphadenopathy was defined as one of the following criteria was fulfilled: (a) size, short diameter was larger than 1 cm (1.5 cm for neck level II); (b) shape, loss of normal coffee bean shape; or (c) presence of necrosis, calcification, or perinodal infiltration. For entire CT images, location of lymphadenopathy, percentage of necrotic lymphadenopathy (necrotic LN_{per}), presence of calcifications, and perinodal infiltration were assessed. Among the necrotic LNs, the LN that had the largest diameter on axial images was selected as the representative LN. For a representative necrotic LN, the maximum diameter, number of necrotic foci, enhancement ratio, shape and margin of LN and necrosis, and degree of necrosis were assayed.

Location of lymphadenopathy was documented based on cervical nodal levels. Necrotic LN_{per} was calculated by formula as follows: number of necrotic lymphadenopathy total number of the cervical lymphadenopathy × 100. In addition, simple visual scoring for necrotic LN_{per} was performed as following criteria: score 1, approximate number of necrotic LNs is < 1/4 of total number of the cervical lymphadenopathy; score 2, number of necrotic LNs is ≥ 1/4 and < 2/4; score 3, necrotic LNs are ≥ 2/4 and < 3/4; score 4, necrotic LNs are ≥ 3/4. Perinodal infiltration was defined as reticular opacities

in perinodal fat or increased perinodal density. Templates used for visual scoring for necrotic lymphadenopathy and perinodal infiltration including schematic figures and imaging samples are shown in Supplementary Figs. 1 and 2.

In analyses for representative necrotic LN, the enhancement ratio was calculated by formula as follows: enhancement ratio = density of solid portion density of necrotic portion (Hounsfield unit, HU). To obtain those densities, a circular region of interest (ROI) was drawn on the solid enhancing and necrotic portions of representative LN. The ROI was drawn to a size of 10.0 mm^2, allowing an error of ± 3 mm^2. It was redrawn if the size of the ROI was larger or smaller than 7–13 mm^2. The evaluators judged the suitability of the ROI size based on the area value presented in the PACS. Degree of necrosis was categorized by simple visual scoring system as follows: score 1, area of necrosis is < 1/4 of whole area of the representative LN; score 2, area of necrosis is ≥ 1/4 and < 2/4; score 3, area of necrosis is ≥ 2/4 and < 3/4; score 4, area of necrosis is ≥ 3/4. Scoring was assessed in a slice that showed the largest necrotic portion. Templates used for the analysis of enhancement ratio, shape and margin of representative LN, shape and margin of necrosis, and degree of necrosis including schematic figures and imaging samples are shown in Supplementary Figs. 3–9.

Statistical analysis

All statistical analyses were performed using SPSS Statistics software, version 22.0 for Windows (IBM Corp.). The data for each parameter were assessed for normality using the Kolmogorov-Smirnov test. In all of the tests, p values < 0.05 were considered statistically significant. All variables were compared in the four groups (metastasis, TL, KD, and lymphoma). Pearson's chi-square test or Fisher's exact test in the software was used to analyze the associations among categorical variables. Kruskal-Wallis H test or one-way ANOVA was performed to compare the ordinal and continuous variables. To assess the reliability of imaging features, weighted kappa and intraclass correlation coefficient (ICC) were used for ordinal and continuous variables. Weighted kappa value of < 0.20, 0.21–0.40, 0.41–0.60, 0.61–0.80, and 0.81–0.10 represented poor, fair, moderate, good, and excellent agreement. ICC values of ≤ 0, 0–0.20, 0.21–0.40, 0.41–0.60, 0.61–0.80, and greater than 0.81 indicated negative, positive but poor, fair, moderate, good, and excellent agreement.

To make a DTA model for the differential diagnoses of cervical necrotic lymphadenopathy, a classification and regression tree (CART) algorithm was used (minimum cases in parent node, 20; minimum cases in child node, 5; maximum tree depth, 5). Two different predictor variable sets ((a) CT imaging alone; (b) CT imaging and clinical information) were used to establish diagnostic trees and those are as follows: (a) CT imaging alone: laterality, necrotic LN_{per} (visual scoring), calcification, perinodal infiltration, tuberculosis in upper lungs, number of necrotic foci, enhancement ratio, shape and margin of representative LN and necrotic portion, and degree of necrosis; (b) CT imaging and clinical information: imaging findings, sex, age, history of underlying malignancy, presence of fever (body temperature ≥ 38 °C), tenderness, and leukocytosis (WBC count ≥ 12,000). To make a DTA model, we used simple visual scoring of the necrotic LN_{per} instead of quantitative data, because intuitive estimation rather than counting is performed in practice. The one-way ANOVA revealed a significant difference in quantitative date of the necrotic LN_{per} among visual scores ($p < 0.001$) (Supplementary Fig. 10). CART analysis was utilized to identify the choice for the best splitting parameters to formulate the diagnostic criteria to differentiate the four diseases. It automatically calculated optimal cutoff points for continuous and ordinal variables. The accuracies of the two diagnostic trees were calculated, and those were validated using the external validation dataset.

Results

Clinical characteristics

The comparison of the clinical characteristics among the four disease groups is summarized in Table 1. Tenderness was most frequently documented in KD (95.1% [58/61]). None of the patients in the metastasis and lymphoma groups presented with tenderness. Out of 90 patients with metastasis, 75 (83.3%) had a known cancer at the time of radiologic report. The types of underlying malignancy for all patients in the metastasis group are summarized in Supplementary Table 1.

Neck CT imaging findings

Table 2 and Fig. 2 summarize the comparison of the CT imaging findings of the four disease groups. Mean necrotic LN_{per} was high in TL (mean ± standard deviation [SD], percent; 85.96 ± 23.15). In visual analysis, score 4 was the most frequently reported in TL (79.7% [51/64]). On the other hand, the lymphoma had a low mean necrotic LN_{per} (mean ± SD, 24.25 ± 18.44), and a large portion of the lymphoma had score 1 in visual analysis (66.7% [22/33]). Perinodal infiltration was frequently demonstrated in KD (80.3% [49/61]), while the other groups showed low rates of perinodal infiltration (TL, 0.0% [0/64]; metastasis, 13.3% [12/90]; lymphoma, 6.1% [2/33]).

In the analysis for representative necrotic LN, the mean size of analyzed LN was 2.20 ± 1.98 cm. Multiple necrotic foci were documented frequently in metastasis (metastasis, 48.9% [44/90]; TL, 3.1% [2/64]; KD, 4.9% [3/61]; lymphoma, 0.0% [0/33]). The mean enhancement ratio was lower than 2.0 only in KD (metastasis, 3.98 ± 5.74; TL, 3.62 ± 3.47; KD, 1.92 ± 0.83; lymphoma, 3.17 ± 3.61). A large portion of the metastasis group showed irregular shape of the LN (8.9% [44/90]). Metastasis

Table 1 Comparisons of clinical characteristics for metastasis, tuberculous lymphadenitis, Kikuchi disease, and lymphoma in training dataset

Diagnosis	Metastasis ($n = 90$)	Tuberculous lymphadenitis ($n = 64$)	Kikuchi disease ($n = 61$)	Lymphoma ($n = 33$)	Total ($N = 248$)	p
Sex						< 0.001
Male	61 (67.8%)	24 (37.5%)	13 (21.3%)	24 (72.7%)	122 (49.2%)	
Female	29 (32.2%)	40 (62.5%)	48 (78.7%)	9 (27.3%)	126 (50.8%)	
Age	57.38 ± 15.36	40.95 ± 15.43	26.57 ± 11.83	61.85 ± 13.99	46.16 ± 19.64	< 0.001
Cancer						< 0.001
Positive	75 (83.3%)	3 (4.7%)	0 (0.0%)	4 (12.1%)	82 (33.1%)	
Negative	15 (16.7%)	61 (95.3%)	61 (100.0%)	29 (87.9%)	166 (66.9%)	
Fever						< 0.001
Positive	0 (0.0%)	7 (10.9%)	22 (36.1%)	1 (3.0%)	30 (12.1%)	
Negative	90 (100.0%)	57 (89.1%)	39 (63.9%)	32 (97.0%)	218 (87.9%)	
Tenderness						< 0.001
Positive	0 (0.0%)	3 (4.7%)	58 (95.1%)	0 (0.0%)	61 (24.6%)	
Negative	90 (100.0%)	61 (95.3%)	3 (4.9%)	33 (100.0%)	187 (75.4%)	
Leukocytosis						0.453
Positive	5 (5.6%)	1 (1.6%)	1 (1.6%)	1 (3.0%)	8 (3.2%)	
Negative	85 (94.4%)	63 (98.4%)	60 (98.4%)	32 (97.0%)	240 (96.8%)	
Protocol of neck CT						< 0.001
Neck CT	51 (56.7%)	64 (100.0%)	61 (100.0%)	31 (93.9%)	207 (83.5%)	
Oropharynx CT	23 (25.6%)	0 (0.0%)	0 (0.0%)	1 (3.0%)	24 (9.7%)	
Larynx CT	13 (14.4%)	0 (0.0%)	0 (0.0%)	0 (0.0%)	13 (5.2%)	
Nasopharynx CT	3 (3.3%)	0 (0.0%)	0 (0.0%)	1 (3.0%)	4 (1.6%)	
Pathologic diagnosis						< 0.001
FNA	33 (36.7%)	25 (39.1%)	10 (16.4%)	1 (3.0%)	69 (27.8%)	
CNB	23 (25.6%)	28 (43.8%)	45 (73.8%)	31 (93.9%)	127 (51.2%)	
Excision	34 (37.8%)	11 (17.2%)	6 (9.8%)	1 (0.0%)	52 (21.0%)	

Data are mean ± standard deviation (SD) for continuous variables and number of patients (%) for nominal variables

FNA, fine needle aspiration; *CNB*, core needle biopsy

and KD frequently showed irregular shape of the necrotic portion (76.7% [69/90] and 85.3% [52/61]). Most of the TL and lymphoma cases had a smooth necrotic margin (95.3% [61/64] and 97.0% [32/33]), while most of the KD cases demonstrated ill-defined necrotic margins (80.3% [49/61]). In the analysis for degree of necrosis, a large portion of TL and lymphoma had a large necrotic area (score 4; 67.2% [43/64] and 81.8% [27/33]). Schematic figures and representative images of four diseases are shown in Fig. 2. Interobserver agreement for imaging features was all good or excellent (Supplementary Table 2).

DTA models

The summary of the two DTA models from imaging alone and imaging with clinical information is shown in Figs. 3 and 4. The models with full information from the CART algorithm are demonstrated in Supplementary Figs. 11 and 12. The accuracies of diagnostic trees from training and validation datasets are shown in Table 3.

In the DTA model by imaging alone, perinodal infiltration, number of necrotic foci, shape of LN, necrotic LN_{per} (score), degree of necrosis, shape and margin of necrotic portion, and enhancement ratio (cutoff value, 1.93) were adopted as significant predictors to discriminate the four diseases. The overall accuracy with 95% confidence interval (CI) was 80.6% (75.2–85.4).

In the DTA model based on imaging findings and clinical information, tenderness, history of underlying malignancy, necrotic LN_{per} (score), degree of necrosis, and number of necrotic foci were selected as significant predictors for differential diagnosis. The overall accuracy was higher than that of the model derived from imaging findings alone (87.1% [95% CI, 82.3–91.0] vs 80.6% [95% CI, 75.2–85.4]).

External validation of the diagnostic tree

Clinical characteristics and imaging findings of the external validation dataset are summarized in Supplementary Tables 3 and 4. The overall diagnostic accuracies with 95% CI in the

Table 2 Comparisons of neck CT imaging findings of metastasis, tuberculous lymphadenitis, Kikuchi disease, and lymphoma in training dataset

Diagnosis	Metastasis ($n = 90$)	Tuberculous lymphadenitis ($n = 64$)	Kikuchi disease ($n = 61$)	Lymphoma ($n = 33$)	Total ($N = 248$)	p
Laterality						0.024
Unilateral	66 (73.3%)	52 (81.3%)	55 (90.2%)	22 (66.7%)	195 (78.6%)	
Bilateral	24 (26.7%)	12 (18.8%)	6 (9.8%)	11 (33.3%)	53 (21.4%)	
Total number of lymph nodes	6.68 ± 6.73	10.86 ± 10.15	10.33 ± 4.86	13.24 ± 8.16	9.53 ± 7.90	< 0.001
Number of necrotic lymph nodes	4.03 ± 5.47	9.69 ± 9.97	2.82 ± 2.53	2.58 ± 1.97	5.00 ± 6.80	< 0.001
Percent of necrotic LN (%), percentage	68.78 ± 34.17	85.96 ± 23.15	31.98 ± 26.90	24.25 ± 18.44	58.24 ± 36.63	< 0.001
Percentage of necrotic LN, score						< 0.001
Score 1	21 (23.3%)	2 (3.1%)	36 (59.0%)	22 (66.7%)	81 (32.7%)	
Score 2	14 (15.6%)	6 (9.4%)	14 (23.0%)	9 (27.3%)	43 (17.3%)	
Score 3	9 (10.0%)	5 (7.8%)	5 (8.2%)	1 (3.0%)	20 (8.1%)	
Score 4	46 (51.1%)	51 (79.7%)	6 (9.8%)	1 (3.0%)	104 (41.9%)	
Calcification						< 0.001
Positive	7 (7.8%)	19 (29.7%)	0 (0.0%)	0 (0.00%)	26 (10.5%)	
Negative	83 (92.2%)	45 (70.3%)	61 (100.0%)	33 (100.00%)	222 (89.5%)	
Perinodal infiltration						< 0.001
Positive	12 (13.3%)	0 (0.0%)	49 (80.3%)	2 (6.1%)	63 (25.4%)	
Negative	78 (86.7%)	64 (100.0%)	12 (19.7%)	31 (94.0%)	185 (74.6%)	
Tuberculosis in upper lung						< 0.001
Positive	5 (5.6%)	23 (35.9%)	0 (0.0%)	1 (3.0%)	29 (11.7%)	
Negative	85 (94.4%)	41 (64.1%)	61 (100.0%)	32 (97.0%)	219 (88.3%)	
Analysis for representative necrotic LN						
Size of analyzed LN (cm)	2.60 ± 2.51	2.22 ± 2.11	1.54 ± 0.52	2.25 ± 1.50	2.20 ± 1.98	< 0.001
Number of necrotic foci						< 0.001
Single	46 (51.1%)	62 (96.9%)	58 (95.1%)	33 (100.0%)	199 (80.2%)	
Multiple	44 (48.9%)	2 (3.1%)	3 (4.9%)	0 (0.0%)	49 (19.8%)	
Density of solid portion, post-CE (HU)	106.26 ± 31.41	99.67 ± 29.37	106.62 ± 18.69	82.45 ± 18.01	101.48 ± 27.69	< 0.001
Density of necrotic portion, post-CE (HU)	38.68 ± 18.64	35.26 ± 12.88	61.86 ± 19.86	32.77 ± 9.95	42.71 ± 20.01	< 0.001
Enhancement ratio	3.98 ± 5.74	3.62 ± 3.47	1.92 ± 0.83	3.17 ± 3.61	3.27 ± 4.18	0.023
Shape of LN						< 0.001
Oval	21 (23.3%)	22 (34.4%)	31 (50.8%)	2 (6.1%)	76 (30.7%)	
Round	25 (27.8%)	24 (37.5%)	29 (47.5%)	27 (81.8%)	105 (42.3%)	
Irregular	44 (48.9%)	18 (28.1%)	1 (1.6%)	4 (12.1%)	67 (27.0%)	
Margin of LN						< 0.001
Smooth	66 (73.3%)	36 (56.3%)	18 (29.5%)	31 (93.9%)	151 (60.9%)	
Ill-defined	24 (26.7%)	28 (43.8%)	43 (70.5%)	2 (6.1%)	97 (39.1%)	
Shape of necrotic portion						< 0.001
Round	21 (23.3%)	35 (54.7%)	9 (14.8%)	27 (81.8%)	92 (37.1%)	
Irregular	69 (76.7%)	29 (45.3%)	52 (85.3%)	6 (18.2%)	156 (62.9%)	
Margin of necrotic portion						< 0.001
Smooth	54 (60.0%)	61 (95.3%)	12 (19.7%)	32 (97.0%)	159 (64.1%)	
Ill-defined	36 (40.0%)	3 (4.7%)	49 (80.3%)	1 (3.0%)	89 (35.9%)	
Degree of necrosis						< 0.001
Score 1	14 (15.6%)	2 (3.1%)	35 (57.4%)	2 (6.1%)	53 (21.4%)	
Score 2	24 (26.7%)	2 (3.1%)	14 (23.0%)	3 (9.1%)	43 (17.3%)	
Score 3	22 (24.4%)	17 (26.6%)	7 (11.5%)	1 (3.0%)	47 (19.0%)	
Score 4	30 (33.3%)	43 (67.2%)	5 (8.2%)	27 (81.8%)	105 (42.3%)	

Data are mean ± standard deviation (SD) for continuous variables and number of patients (%) for nominal variables

Percent of necrotic lymph node (%, quantitative data) = number of necrotic lymphadenopathy / total number of the cervical lymphadenopathy × 100

Percentage of necrotic lymph node (LN) (visual scoring): score 1, approximate number of necrotic LNs is < 1/4 of total number of the cervical lymphadenopathy; score 2, number of necrotic LNs is ≥ 1/4 and < 2/4; score 3, necrotic LNs are ≥ 2/4 and < 3/4; score 4, necrotic LNs are ≥ 3/4

Enhancement ratio = density of solid portion / density of necrotic portion (Hounsfield unit)

Degree of necrosis: score 1, area of necrosis is < 1/4 of whole area of the representative LN; score 2, area of necrosis is ≥ 1/4 and < 2/4; score 3, area of necrosis is ≥ 2/4 and < 3/4; score 4, area of necrosis is ≥ 3/4

LN, lymph nodes; *CE*, contrast-enhanced; *HU*, Hounsfield unit

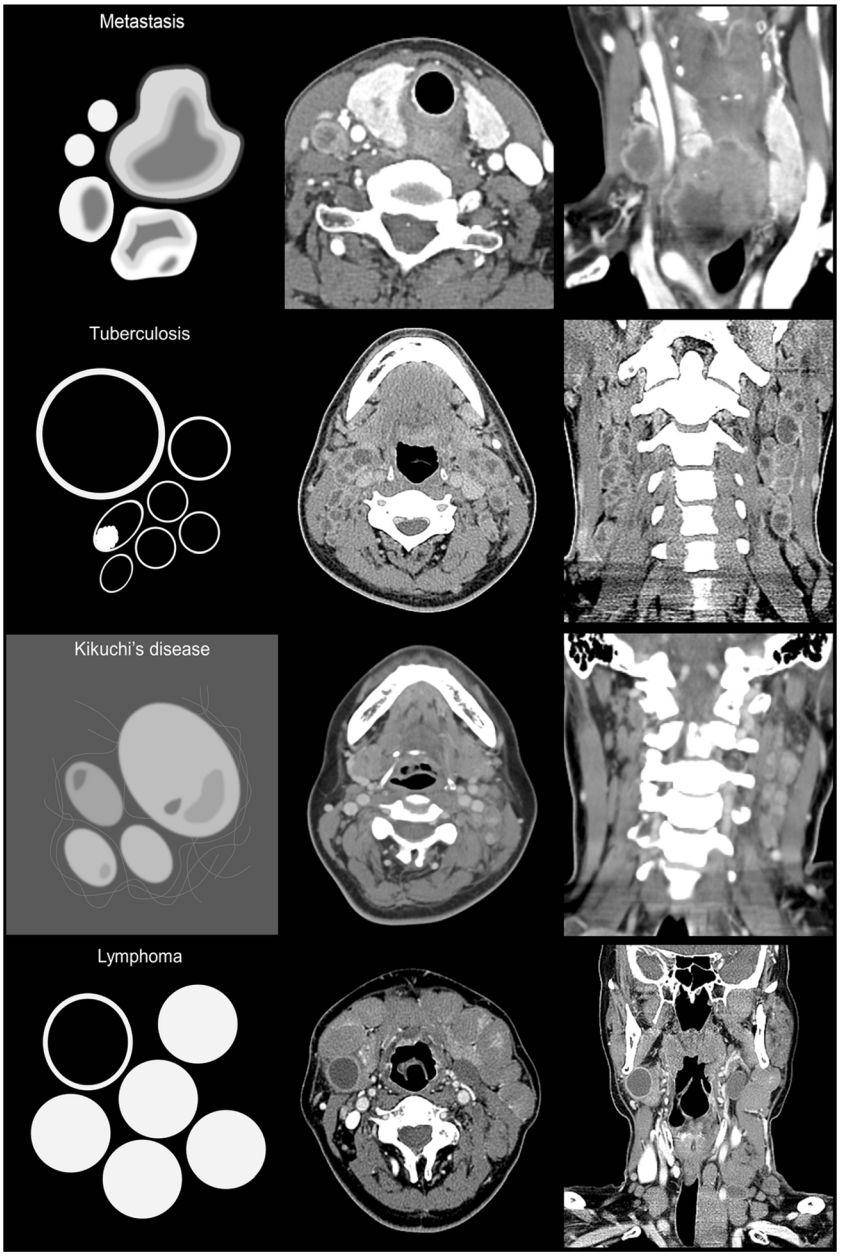

Fig. 2 Schematic figures and representative computed tomography images in patients with metastatic lymphadenopathy, tuberculous lymphadenitis, Kikuchi disease, or lymphoma. *First row*: Images of a 62-year-old woman with metastasis from anaplastic thyroid cancer proven via excisional biopsy. Two out of two lymphadenopathies show necrosis. Representative LN demonstrates multiple necrotic foci and irregular-shaped ill-defined necrotic portion. *Second row*: Images of a 30-year-old man with tuberculous lymphadenitis proven by core needle biopsy. Most of the lymphadenopathies show necrosis (percentage of necrosis; quantitative analysis, 93.3% [43/45]; visual scoring, score 4). Representative lymph node (LN) shows smooth margin of necrotic portion and high degree of necrosis (score 4). *Third row*: Images of a 37-year-old woman with Kikuchi disease proven by core needle biopsy. Prominent perinodal infiltration is observed. Representative LN shows small necrotic portion (degree of necrosis, score 2). The necrotic portion is not well distinguished from the solid portion because the density of the necrotic portion is relatively high (enhancement ratio = 113 HU/69 HU = 1.638). *Bottom row*: Images of a 72-year-old man with diffuse large B cell lymphoma proven by core needle biopsy. Percentage of necrosis was low (quantitative analysis, 17.4% [4/23]; visual scoring, score 1). Representative LN shows large necrotic portion (degree of necrosis, score 4) and smooth inner margin

external validation datasets ($N = 42$; 25 men and 17 women; mean age, 46.19 ± 18.56 years; range, 9–75 years) were 73.8% (58.0–86.1) and 88.1% (74.4–96.0) with imaging alone and imaging with clinical findings, respectively.

Discussion

In the present study, perinodal infiltration, number of necrotic foci, shape of LN, necrotic LN_{per} (score), degree of necrosis,

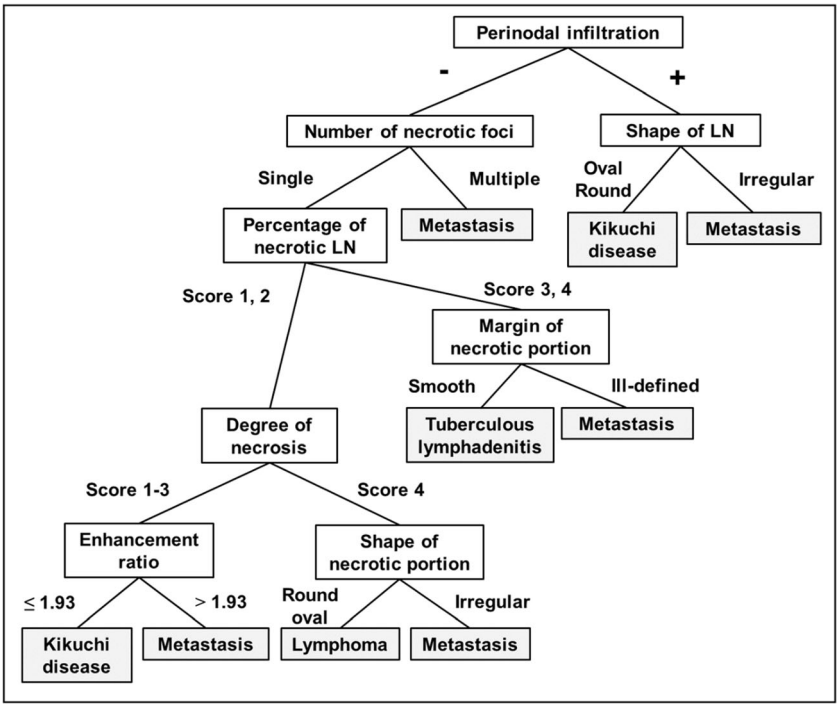

Fig. 3 Diagnostic tree derived from imaging findings. Percentage of necrotic lymph node (LN): score 1, approximate number of necrotic LNs is < 1/4 of total number of the cervical lymphadenopathy; score 2, number of necrotic LNs is ≥ 1/4 and < 2/4; score 3, necrotic LNs are ≥ 2/4 and < 3/4; score 4, necrotic LNs are ≥ 3/4. Enhancement ratio = density of solid portion / density of necrotic portion (Hounsfield unit). Degree of necrosis: score 1, area of necrosis is < 1/4 of whole area of the representative LN; score 2, area of necrosis is ≥ 1/4 and < 2/4; score 3, area of necrosis is ≥ 2/4 and < 3; score 4, area of necrosis is ≥ 3/4

shape and margin of necrotic portion, and enhancement ratio (cutoff value, 1.93) were significant imaging criteria to discriminate metastasis, TL, KD, and lymphoma. The overall accuracies of the diagnostic tree consisted of the eight imaging findings were 80.6% in the training dataset and 73.8% in the validation dataset. Diagnostic accuracy was enhanced by adding clinical information such as tenderness and history of underlying malignancy (87.1%).

Metastasis is the main cause of cervical necrotic lymphadenopathy. Various size criteria for discrimination of metastatic LNs have been suggested [5, 15–17], and the loss of a coffee bean shape or the central fatty hilum and necrosis are well-known imaging features indicating metastasis [1, 5, 18, 19]. Among them, necrosis is a specific imaging feature of metastatic lymphadenopathy. The general mechanism of necrosis in metastatic LNs is a destruction of the normal vascular

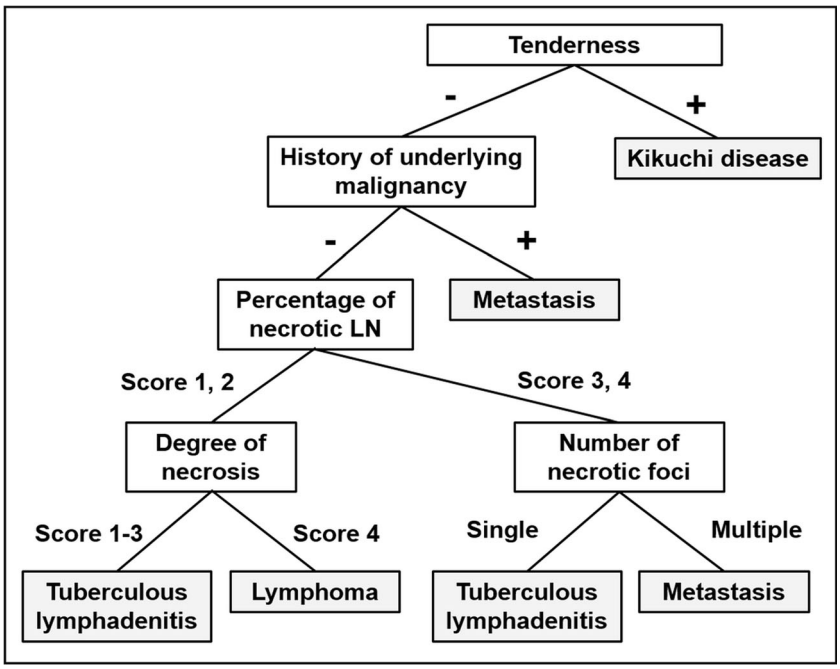

Fig. 4 Diagnostic tree derived from imaging findings and clinical information. Percentage of necrotic lymph node (LN): score 1, approximate number of necrotic LNs is < 1/4 of total number of the cervical lymphadenopathy; score 2, number of necrotic LNs is ≥ 1/4 and < 2/4; score 3, necrotic LNs are ≥ 2/4 and < 3/4; score 4, necrotic LNs are ≥ 3/4. Degree of necrosis: score 1, area of necrosis is < 1/4 of whole area of the representative LN; score 2, area of necrosis is ≥ 1/4 and < 2/4; score 3, area of necrosis is ≥ 2/4 and < 3; score 4, area of necrosis is ≥ 3/4

Table 3 Diagnostic Performance of Diagnostic Trees

			Prediction				
		Diagnosis	Metastasis	Tuberculous lymphadenitis	Kikuchi disease	Lymphoma	Accuracy (%)
Imaging findings	Training Dataset	Metastasis ($n = 90$)	71	14	5	0	78.9
		Tuberculosis ($n = 64$)	11	51	1	1	79.7
		Kikuchi disease ($n = 61$)	4	1	56	0	91.8
		Lymphoma ($n = 33$)	4	2	5	22	66.7
		Overall ($N = 248$)					80.6
	External validation dataset	Metastasis ($n = 20$)	14	3	2	1	70.0
		Tuberculosis ($n = 9$)	2	7	0	0	77.8
		Kikuchi disease ($n = 10$)	2	0	8	0	80.0
		Lymphoma ($n = 3$)	1	0	0	2	66.7
		Overall ($N = 42$)					73.8
Imaging finding and clinical information	Training dataset	Metastasis ($n = 90$)	80	10	0	0	88.9
		Tuberculosis ($n = 64$)	4	56	3	1	87.5
		Kikuchi disease ($n = 61$)	0	3	58	0	95.1
		Lymphoma ($n = 33$)	4	7	0	22	66.7
		Overall ($N = 248$)					87.1
	External validation dataset	Metastasis ($n = 20$)	19	1	0	0	95.0
		Tuberculosis ($n = 9$)	2	6	1	0	66.7
		Kikuchi disease ($n = 10$)	0	0	10	0	100.0
		Lymphoma ($n = 3$)	0	1	0	2	66.7
		Overall ($N = 42$)					88.1

structure of the LNs by tumor cells and replacement by neovascularized blood vessels that are unable to provide sufficient blood flow. If the rate of neovascularization is slower than that of the cancer cell growth, necrosis occurs [20]. In our study, the DTA model based on the imaging alone and that with clinical information, metastasis had an accuracy of approximately 79% and 89%. Despite various imaging features, metastasis could be differentiated from the other diseases by several characteristic features like irregular shape of the LN, multiple necrotic foci, and ill-defined and irregular-shaped necrotic portion.

Perinodal infiltration (80%) was very common in KD, in line with previous studies [12, 13, 21, 22]. Pathologically, the perinodal infiltration on CT corresponds to periadenitis. It is caused by infiltration of inflammatory cells and karyorrhectic debris (the destructive fragmentation of the nucleus of dying histiocytes and plasmacytoid monocytes) around the LN through the LN capsule broken by inflammation [23]. One potential explanation is that the paracortical location of coagulative necrosis of KD may destroy the LN capsule [23]. However, perinodal infiltration could also be observed in metastatic lymphadenopathy with extracapsular extension. Thus, it is possible to misclassify metastasis and KD using only the CT-based model.

The necrotic LN_{per} was a significant predictor for differential diagnosis. Out of all TL, 89% demonstrated necrosis in more than half of all the cervical lymphadenopathy. On the other hand, 0% of the lymphoma and 20% of KD had necrosis in more than half of all the cervical lymphadenopathy. These results for TL and KD are in close agreement with previous studies [12, 13, 21], and there has been no study reporting the necrotic LN_{per} in lymphoma. There are three potential explanations for these results. First, in TL, early extensive caseous necrosis with tissue destruction by mycobacterium leads to necrosis in most LN. Second, there are three stages in KD (proliferative, necrotizing, and xanthomatous stages), and necrosis is detected by CT at the necrotizing stage in association with symptoms like fever and tenderness. Not all LNs are at the same stage and only a small number are necrotic. Third, in lymphoma, the potential mechanism of extensive necrosis is the occlusion of the supplying hilar artery by the tumor (compression or invasion) in addition to lymphatic flow obstruction [24, 25]. This phenomenon occurs mostly in the patients with poor prognosis [26].

The degree of necrosis provided important information for the differential diagnosis of the four diseases. The representative LN in TL and lymphoma demonstrated extensive central necrosis with rim enhancing solid portion.

Aggressive caseous necrosis by mycobacterium (TL) and extensive ischemic cell necrosis by hilar arterial occlusion (lymphoma) are potential mechanisms [25]. Although the degree of necrosis in KD varies, microscopic coagulative necrosis is more common than overt macroscopic necrosis in the early stage of disease [27–29]. Thus, the necrotic foci in LN are generally small.

The median enhancement ratio was lower than 2.0 only in KD. A low enhancement ratio implies that the attenuation of the necrotic portion is high. Necrotic foci in TL, metastasis, and lymphoma are "true necrosis" composed of non-cellular materials, while those of KD are not [12, 13, 21, 22, 30]. The paracortical coagulative necrosis of KD consists of prominent karyorrhectic debris and eosinophilic fibrinoid deposits [13, 29]. Additionally, the high density of necrotic foci is accentuated by the water loss due to cytoplasm concentration and protein denaturation [13, 31]. Thus, KD should be considered if necrotic foci are not well differentiated from the solid portion.

Several other imaging modalities have been evaluated to differentiate cervical necrotic lymphadenopathies. Although accuracy for detecting necrosis is highest in CT compared with that of MR or US [1, 18], previous studies reported on the usefulness of MR and US as follows. With MR, metastatic LNs demonstrate higher pure water diffusion values and diffusion heterogeneity than nonmetastatic LNs [17]. The necrotic portion of TL shows high signal intensity on diffusion-weighted image, and conversely hypointensity in lymphoma and metastasis [2]. The ADC of the necrotic portion is higher in metastasis than in TL [4]. ADC of the necrotic portion in suppurative lymphadenitis is lower than that in metastasis and lymphoma [3]. In addition, the necrotic portion of KD shows a low signal intensity on T2-weighted images than that of metastasis or TL [22]. Regarding US, over 76% of LNs in the patients with KD demonstrate increased echogenicity in the perinodal area, and TL shows a hypoechoic necrotic portion more frequently than KD on US (71% vs 9%) [6].

Our study has several limitations. First, it is a retrospective study with a limited number of patients. Although we reviewed all radiologic reports of CT, patients were excluded in this study if the radiologist who first interprets the CT did not mention necrosis in the report. Moreover, no pathological correlation with imaging features was done. Second, in our study, the prevalence of TL and KD was higher than that in the general Western population. The overall diagnostic accuracy may be different in that population. Third, other nodal diseases that could exhibit necrosis were not included in the diagnostic tree. In our study, among all the patients with the necrotic LNs, the presumptive diagnosis was suppurative lymphadenitis in five pediatric patients, and systemic lupus erythematosus–associated lymphadenitis in two patients. However, the pathologic diagnosis was not confirmed in those patients. Fourth, external validation was performed using only the CT that was obtained at our hospital. However, CT is a very standardized technique and it is unlikely that significant differences could be observed in other centers. Fifth, we performed the analysis for the representative necrotic LN in one slice, not a volumetric analysis. The characteristics of the entire LN may not be reflected in this analysis. Finally, we analyzed CT image with a fixed window setting for consistent image analysis between observers. This is somewhat different from the general practice because a narrower window setting is generally applied to detect necrotic tissue portions.

In conclusion, the DTA model based on simple CT imaging findings and basic clinical information showed a high accuracy for discriminating metastasis, TL, KD, and lymphoma. This model may be helpful for differential diagnosis of the patients with cervical necrotic lymphadenopathy.

Funding The authors state that this work has not received any funding.

Compliance with ethical standards

Guarantor The scientific guarantor of this publication is Byungjun Kim.

Conflict of interest The authors of this manuscript declare no relationships with any companies whose products or services may be related to the subject matter of the article.

Statistics and biometry One of the authors has significant statistical expertise.

Informed consent Written informed consent was waived by the Institutional Review Board.

Ethical approval Institutional Review Board approval was obtained.

Methodology
- retrospective
- diagnostic or prognostic study
- performed at one institution

References

1. King AD, Tse GM, Ahuja AT et al (2004) Necrosis in metastatic neck nodes: diagnostic accuracy of CT, MR imaging, and US. Radiology 230:720–726
2. Koç O, Paksoy Y, Erayman I, Kivrak AS, Arbag H (2007) Role of diffusion weighted MR in the discrimination diagnosis of the cystic and/or necrotic head and neck lesions. Eur J Radiol 62:205–213
3. Kato H, Kanematsu M, Kato Z et al (2013) Necrotic cervical nodes: usefulness of diffusion-weighted MR imaging in the differentiation of suppurative lymphadenitis from malignancy. Eur J Radiol 82: e28–e35
4. Zhang Y, Chen J, Shen J, Zhong J, Ye R, Liang B (2013) Apparent diffusion coefficient values of necrotic and solid portion of lymph

nodes: differential diagnostic value in cervical lymphadenopathy. Clin Radiol 68:224–231
5. Eisenmenger LB, Wiggins RH 3rd (2015) Imaging of head and neck lymph nodes. Radiol Clin North Am 53:115–132
6. Ryoo I, Suh S, Lee YH, Seo HS, Seol HY (2015) Comparison of ultrasonographic findings of biopsy-proven tuberculous lymphadenitis and Kikuchi disease. Korean J Radiol 16:767–775
7. Han F, Xu M, Xie T et al (2018) Efficacy of ultrasound-guided core needle biopsy in cervical lymphadenopathy: a retrospective study of 6,695 cases. Eur Radiol 28:1809–1817
8. Baek CH, Kim SI, Ko YH, Chu KC (2000) Polymerase chain reaction detection of mycobacterium tuberculosis from fine-needle aspirate for the diagnosis of cervical tuberculous lymphadenitis. Laryngoscope 110:30–34
9. Mittal P, Handa U, Mohan H, Gupta V (2011) Comparative evaluation of fine needle aspiration cytology, culture, and PCR in diagnosis of tuberculous lymphadenitis. Diagn Cytopathol 39:822–826
10. Lin HC, Su CY, Huang CC, Hwang CF, Chien CY (2003) Kikuchi's disease: a review and analysis of 61 cases. Otolaryngol Head Neck Surg 128:650–653
11. Kucukardali Y, Solmazgul E, Kunter E, Oncul O, Yildirim S, Kaplan M (2007) Kikuchi–Fujimoto disease: analysis of 244 cases. Clin Rheumatol 26:50–54
12. Baek HJ, Lee JH, Lim HK, Lee HY, Baek JH (2014) Diagnostic accuracy of the clinical and CT findings for differentiating Kikuchi's disease and tuberculous lymphadenitis presenting with cervical lymphadenopathy. Jpn J Radiol 32:637–643
13. Lee S, Yoo JH, Lee SW (2012) Kikuchi disease: differentiation from tuberculous lymphadenitis based on patterns of nodal necrosis on CT. AJNR Am J Neuroradiol 33:135–140
14. Holzapfel K, Duetsch S, Fauser C, Eiber M, Rummeny EJ, Gaa J (2009) Value of diffusion-weighted MR imaging in the differentiation between benign and malignant cervical lymph nodes. Eur J Radiol 72:381–387
15. Atula TS, Varpula MJ, Kurki TJ, Klemi PJ, Grénman R (1997) Assessment of cervical lymph node status in head and neck cancer patients: palpation, computed tomography and low field magnetic resonance imaging compared with ultrasound-guided fine-needle aspiration cytology. Eur J Radiol 25:152–161
16. Chong V (2004) Cervical lymphadenopathy: what radiologists need to know. Cancer Imaging 4:116
17. Wu Q, Zheng D, Shi L, Liu M, Wang M, Shi D (2017) Differentiating metastatic from nonmetastatic lymph nodes in cervical cancer patients using monoexponential, biexponential, and stretched exponential diffusion-weighted MR imaging. Eur Radiol 27:5272–5279
18. Yousem DM, Som PM, Hackney DB, Schwaibold F, Hendrix RA (1992) Central nodal necrosis and extracapsular neoplastic spread in cervical lymph nodes: MR imaging versus CT. Radiology 182: 753–759
19. van den Brekel MW (2000) Lymph node metastases: CT and MRI. Eur J Radiol 33:230–238
20. Cui QL, Yin SS, Fan ZH, Yang W, Wang S, Yan K (2018) Diagnostic value of contrast-enhanced ultrasonography and time-intensity curve in differential diagnosis of cervical metastatic and tuberculous lymph nodes. J Ultrasound Med 37:83–92
21. Kwon SY, Kim TK, Kim YS, Lee KY, Lee NJ, Seol HY (2004) CT findings in Kikuchi disease: analysis of 96 cases. AJNR Am J Neuroradiol 25:1099–1102
22. Na DG, Chung TS, Byun HS, Kim HD, Ko YH, Yoon JH (1997) Kikuchi disease: CT and MR findings. AJNR Am J Neuroradiol 18: 1729–1732
23. Onciu M, Medeiros LJ (2003) Kikuchi-Fujimoto lymphadenitis. Adv Anat Pathol 10:204–211
24. Tilak SP, Howard JM (1964) The influence of the dual circulation on the viability of lymph nodes following interruption of their blood or lymphatic supply. Surg Gynecol Obstet 119:349–352
25. Saito A, Takashima S, Takayama F, Kawakami S, Momose M, Matsushita T (2001) Spontaneous extensive necrosis in non-Hodgkin lymphoma: prevalence and clinical significance. J Comput Assist Tomogr 25:482–486
26. Adams HJA, De Klerk JMH, Fijnheer R, Dubois SV, Nievelstein RAJ, Kwee TC (2015) Prognostic value of tumor necrosis at CT in diffuse large B-cell lymphoma. Eur J Radiol 84:372–377
27. Chamulak GA, Brynes RK, Nathwani BN (1990) Kikuchi-Fujimoto disease mimicking malignant lymphoma. Am J Surg Pathol 14:514–523
28. Dorfman RF, Berry GJ (1988) Kikuchi's histiocytic necrotizing lymphadenitis: an analysis of 108 cases with emphasis on differential diagnosis. Semin Diagn Pathol 5:329–345
29. Bosch X, Guilabert A, Miquel R, Campo E (2004) Enigmatic Kikuchi-Fujimoto disease: a comprehensive review. Am J Clin Pathol 122:141–152
30. Kim KN, Kim DW, Kim HJ, Park JH, Kim CS, Kim HS (1999) CT findings of Kikuchi disease: correlation with pathologic findings. J Korean Radiol Soc 41:879–884
31. Kato H, Kanematsu M, Kato Z et al (2011) MR imaging findings of cervical lymphadenopathy in patients with Kikuchi disease. Eur J Radiol 80:e576–e581